Magneto-Elastic Coupling in a Sinusoidal Modulated Magnet Cr_2GaN

Hui-Can Mao(毛慧灿)[1,2], Yu-Feng Li(李玉峰)[3], Qing-Yong Ren(任清勇)[4,5], Mi-Hai Chu(褚密海)[6], Helen E. Maynard-Casely[7], Franz Demmel[8], Devashibhai Adroja[8], Hai-Hu Wen(闻海虎)[3], Yin-Guo Xiao(肖荫果)[6*], and Hui-Qian Luo(罗会仟)[1,9*]

[1]*Beijing National Laboratory for Condensed Matter Physics, Institute of Physics, Chinese Academy of Sciences, Beijing 100190, China*
[2]*University of Chinese Academy of Sciences, Beijing 100049, China*
[3]*National Laboratory of Solid State Microstructures and Department of Physics, Collaborative Innovation Center of Advanced Microstructures, Nanjing University, Nanjing 210093, China*
[4]*Institute of High Energy Physics, Chinese Academy of Sciences, Beijing 100049, China*
[5]*Spallation Neutron Source Science Center, Dongguan 523803, China*
[6]*School of Advanced Materials, Shenzhen Graduate School, Peking University, Shenzhen 518055, China*
[7]*Australian Centre for Neutron Scattering, Australian Nuclear Science and Technology Organisation, Lucas Heights NSW-2232, Australia*
[8]*ISIS Facility, Rutherford Appleton Laboratory, Chilton, Didcot Oxon OX11 0QX, United Kingdom*
[9]*Songshan Lake Materials Laboratory, Dongguan 523808, China*

(Received 28 June 2022; accepted manuscript online 27 July 2022)

We use neutron powder diffraction to investigate the magnetic and crystalline structure of Cr_2GaN. A magnetic phase transition is identified at $T \approx 170$ K, whereas no trace of structural transition is observed down to 6 K. Combining Rietveld refinement with irreducible representations, the spin configuration of Cr ions in Cr_2GaN is depicted as an incommensurate sinusoidal modulated structure characterized by a propagating vector $k = (0.365, 0.365, 0)$. Upon warming up to the paramagnetic state, the magnetic order parameter closely resembles to the temperature dependence of c-axis lattice parameter, suggesting strong magneto-elastic coupling in this compound. Therefore, Cr_2GaN provides a potential platform for exploration of magnetically tuned properties such as magnetoelectric, magnetostrictive and magnetocaloric effects, as well as their applications.

DOI: 10.1088/0256-307X/39/9/097501

The $M_{n+1}AX_n$ (MAX) phases, crystallized in hexagonal $P6_3/mmc$, where M is a transition metal element, A is an ⅢA or ⅣA group element, X is either C or N and n varies from 1 to 3, have attracted considerable interest for a unique combination of metallic properties such as good electrical conductivity, and ceramic properties like high elastic moduli.[1–3] The MAX compounds are composed of near-close-packed layers of M_6X octahedra interleaved with layers of pure A atoms. These MAX phases are extremely resistant to oxidation and thermal shock, elastically stiff, while at the same time they exhibit high electrical and thermal conductivity which are machinable.[4,5] In addition to the unique metallic and ceramic characters in inherently nanolaminated MAX phases, magnetism characterized by high stability and tunable anisotropic properties are fascinating for both fundamental materials science and practical applications, such as spintronics manipulated by the interlayer exchange coupling, and metallic magnetism realized in the geometrically frustrated two-dimensional plane.[6–10]

Mostly magnetic MAX phases reported to date, either in bulk or thin film form, are composed of Cr or Mn as transition metal elements.[6] The significantly correlated nature of the d orbitals of Cr and Mn in MAX compounds generates diverse magnetic interactions under either ferromagnetic (FM) or antiferromagnetic (AFM) order, which strongly depend on the chemical composition and other tuning parameters such as temperature and pressure. For example, Cr_2GeC is probably located in the vicinity of an FM quantum critical point, whereas the Mn-doped Cr_2GeC shows itinerant-electron ferromagnetism in a wide range of the degree of electron localization.[11] Interestingly, Mn_2GaC undergoes a magnetic transition (∼210 K) from a collinear AFM state to a non-collinear AFM configuration due to the spin reorientation, accompanied by a c-axis lattice compression with decreasing temperature.[7,8] This suggests a strong coupling between spin and lattice, so called "magneto-elastic" coupling, in the layered MAX phase. Such rich magnetic properties in MAX phases open a pathway to explore new functionalities for spintronic, magnetoelectric and magnetocaloric applications by enabling the manipulation of electronic, magnetic and crystalline structure.

Analogously, a spin-density-wave (SDW) transition has been found in MAX phase Cr_2GaN at $T_N = 170$ K by measuring the zero-field muon spin relaxation (ZF-μSR), magnetic susceptibility and resistivity.[12,13] Furthermore, nuclear magnetic resonance (NMR) experiments suggest that the static and distributed internal field is expected for the frustrated magnetism or incommensurate SDW state[13] in Cr_2GaN. Such rich and complicated magnetic properties in Cr_2GaN will inspire us to determine its mag-

*Corresponding authors. Email: y.xiao@pku.edu.cn; hqluo@iphy.ac.cn
© 2022 Chinese Physical Society and IOP Publishing Ltd

netic ground state and further to explore the interactions between spin and lattice by neutron diffraction experiments.

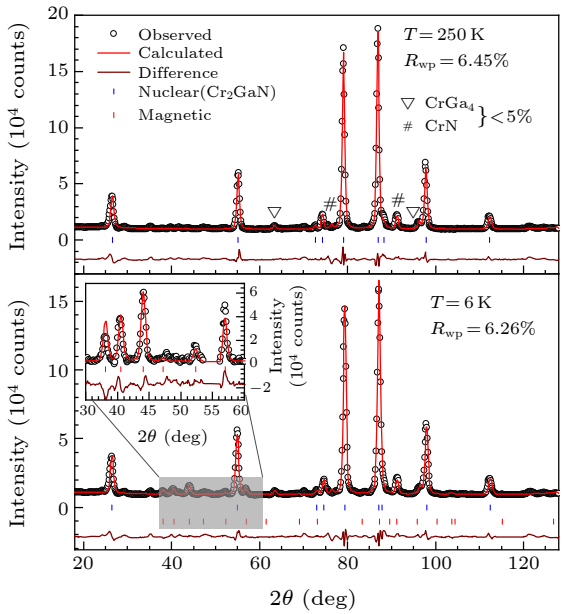

Fig. 1. The Rietveld refinement results with hexagonal phase $P6_3/mmc$ at (a) 250 K and (b) 6 K. The vertical blue lines represent the positions of the Bragg peaks in Cr_2GaN, red lines designate those of magnetic peaks, inverted triangle is the impurities of $CrGa_4$ and CrN. The inset in Fig. 1(b) gives a schematic show of the refinement of magnetic phase in the range of $2\theta \sim 35°$–$60°$.

The polycrystalline samples of Cr_2GaN were synthesized by the solid state reaction method as described in Ref. [12]. Neutron powder diffraction experiments were carried out on both OSIRIS high-resolution diffractometer at ISIS facility, STFC Rutherford Appleton Laboratory (Proposal No. RB1610019) and WOMBAT high-intensity diffractometer at Australian Nuclear Science and Technology Organisation (Proposal No. P6014) with wavelength $\lambda = 2.95$ Å. To obtain diffraction data with good counting statistics and homogeneous background, about 5 g of Cr_2GaN powders were laid flat between two layers of aluminum foil, then rolled up and placed against the wall of Aluminum can for the experiment at OSIRIS diffractometer, whereas the same batch of samples ∼5 g were sealed in a vanadium can at WOMBAT diffractometer. The full pattern measurements were conducted on WOMBAT diffractometer at 6 K and 250 K by covering the scattering angle 2θ from 15° to 136°, whereas the temperature-dependent diffraction data ranging from 10 K to 250 K were collected at OSIRIS diffractometer with interplanar d-spacing from 3.1 to 5.3 Å, including a nuclear reflection (004) and several magnetic reflections. For the structural refinement, we focus on the WOMBAT data using Rietveld method and irreducible representation theory embedded in the FullProf[14,15] and SARAH[16] software package.

The raw data of neutron diffraction patterns at 250 K and 6 K obtained from WOMBAT diffractometer are presented in Fig. 1. To quantitatively analyze the crystal structure and magnetic structure of Cr_2GaN, we have performed the Rietveld refinement for these two data sets. The majority of Bragg reflections can be indexed by a hexagonal phase of Cr_2GaN with space group $P6_3/mmc$ for both patterns at 250 K and 6 K, whereas some weak reflections indicate the existence of very small amounts of $CrGa_4$ and CrN impurity phases (<5%) [Fig. 1(a)]. The parameters for the quality of this two fittings, including profile factor R_p and weighted profile factor R_{wp}, are 4.75(3), 6.44(5) at 250 K and 4.88(4), 6.45(3) at 6 K, respectively. All crystallographic parameters listed in Table 1 are mostly consistent with the previous x-ray diffraction results.[12] Since both data sets at 250 K and 6 K can be fully identified with the same space group $P6_3/mmc$, we thus conclude that there is no observable structural phase transition in Cr_2GaN down to 6 K. As illustrated in Fig. 1(b), a few magnetic peaks emerge at low temperature of 6 K ranging from 35° to 60°, indicating the formation of a long-rang magnetic order in Cr_2GaN. All magnetic peaks at 6 K can be well indexed with a propagation vector $k = (0.365, 0.365, 0)$, suggesting an incommensurate magnetic structure.

Table 1. Crystallographic data of Cr_2GaN at 250 K and 6 K.

		250 K		6 K
Space group		$P6_3/mmc$		$P6_3/mmc$
a (Å)		2.861(5)		2.850(1)
c (Å)		12.671(9)		12.713(1)
z_{Cr}		0.087(2)		0.089(1)
B_{iso}(Cr) (Å^2)		1.118(2)		0.350(1)
B_{iso}(Ga) (Å^2)		0.839(2)		0.515(8)
B_{iso}(N) (Å^2)		1.112(6)		0.960(8)
Atom	Wyckoff	x	y	z
Cr	$4f$	1/3	2/3	z_{Cr}
Ga	$2d$	1/3	2/3	0.75
N	$2a$	0	0	0

The magnetic symmetry analysis for Cr_2GaN is performed using the program SARAH, by which the allowed symmetry coupling in the form of irreducible representation (IR) and their basis vectors (BVs) can be obtained. With the incommensurate magnetic propagation vector $k = (0.365, 0.365, 0)$, the Cr ion occupying at crystallographic Wyckoff site ($4f$) has four one-dimensional irreducible magnetic representations including Γ_1, Γ_2, Γ_3 and Γ_4, and each of them has three basis vectors with only real components. To determine the magnetic structure of Cr_2GaN, we use all possible IRs in the magnetic structural model to fit the neutron diffraction pattern at 6 K.

We find that irreducible representation Γ_3 is the best fitting of all magnetic peaks, whereas the other three representations can be excluded due to poor fits of magnetic peaks. The decomposition of the magnetic representation Γ_3 is given in Table 2. According to Γ_3, the Cr moments are ordered in a sinusoidal structure in the magnetic unit cell and the refined vector components of the magnetic moment are $m_x = 0.4\,\mu_B$, $m_y = -0.05\,\mu_B$ and $m_z = 1.5\,\mu_B$. The Cr ion at $4f$ Wyckoff site has 4 equivalent Cr ions in the unit cell marked with Cr1(0.333, 0.667, 0.089), Cr2(0.667, 0.333, 0.911), Cr3(0.333, 0.667, 0.411), and Cr4(0.667, 0.333, 0.589) in Fig. 2(a), and their (m_x, m_y, m_z) are $(0.4, -0.05, 1.5)\,\mu_B$, $(0.05, -0.4, 1.5)\,\mu_B$, $(-0.4, 0.05, 1.5)\,\mu_B$, and $(-0.05, 0.4, 1.5)\,\mu_B$, respectively. It is clear that the magnetic moment components of Cr

ions are lying in a–c and b–c planes. More precisely, we note that Cr1 and Cr3 moments in a–c plane (or Cr2 and Cr4 in b–c plane) form a sinusoidal wave modulated structure model along a-axis (or b-axis) as shown in Figs. 2(b) and 2(c), respectively. The estimated value of the total ordered moment is about $1.56\mu_B$, which is slightly larger than the reported results of μSR experiments ($< 1\mu_B$).[13]

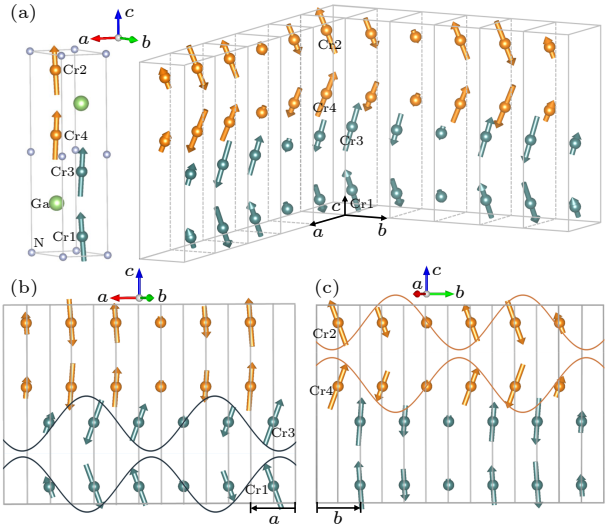

Fig. 2. (a) Three-dimensional sinusoidal modulated magnetic structure of Cr_2GaN at 6 K in single unit cell and supercell. Two-dimensional sinusoidal modulated magnetic structure of Cr_2GaN at 6 K along (b) a-axis and (c) b-axis.

Table 2. Nonzero basis vectors (BVs) of the irreducible representations (IRs) and positional coordinates for Cr atoms that are used to describe the sinusoidal modulated magnetic structure of Cr_2GaN with space group $P6_3/mmc$ and propagation vector $k = (0.365, 0.365, 0)$.

			BV components			Positional coordinates		
IR	BV	Atom	$m_{\|\|a}$	$m_{\|\|b}$	$m_{\|\|c}$	x	y	z
Γ_3	ψ_7	1	1	0	0	x	y	z
		2	0	−1	0	$\bar{x}$+1	$\bar{y}$+1	$\bar{z}$+1
		3	−1	0	0	x	y	$\bar{z}+1/2$
		4	0	1	0	$\bar{x}$+1	$\bar{y}$+1	$z+1/2$
	ψ_8	1	0	1	0	x	y	z
		2	−1	0	0	$\bar{x}$+1	$\bar{y}$+1	$\bar{z}$+1
		3	0	−1	0	x	y	$\bar{z}+1/2$
		4	1	0	0	$\bar{x}$+1	$\bar{y}$+1	$z+1/2$
	ψ_9	1	0	0	1	x	y	z
		2	0	0	1	$\bar{x}$+1	$\bar{y}$+1	$\bar{z}$+1
		3	0	0	1	x	y	$\bar{z}+1/2$
		4	0	0	1	$\bar{x}$+1	$\bar{y}$+1	$z+1/2$

Now we turn to the diffraction pattern covering interplanar distance $d \sim 3.1$–4.65 Å as shown in Fig. 3, obtained from OSIRIS diffractometer with measured temperatures range from 10 K to 250 K. In Fig. 3(a), the four magnetic peaks $(002)_M \pm k$, $(000)_M \pm k$, $(101)_M - k$, and $(100)_M - k$, centered around 3.32 Å, 3.85 Å, 4.28 Å, and 4.48 Å, gradually become weaker with increasing temperature and disappear completely above magnetic phase transition temperature $T_M \approx 170$ K. Notably, the positions of all magnetic peaks shift upon warming up to T_M, so does the position of (004) nuclear peak. As both the magnetic and crystalline structures keep the same below T_M, the peak shift of (004) toward smaller d indicates that the lattice parameter c also decreases. The lattice parameter c in Fig. 3(b) obtained from OSIRIS diffractometer is slightly larger than that in Table 1 obtained from WOMBAT diffractometer, which are mainly attributed to the difference between the two diffractometers. The order parameter of the sinusoidal magnetism can be represented by the normalized intensities of two magnetic peaks $(101)_M - k$ and $(000)_M \pm k$, which are plotted together with the lattice constant c in Fig. 3(b) for comparison. Surprisingly, all these parameters decrease simultaneously in a uniform manner with increasing temperature until a kink occurs at 170 K, in perfect agreement with the transition temperature reported previously.[12,13] The analogous temperature-dependent behavior in the wide temperature range from 10 K to 250 K for the normalized intensity of magnetic peaks and lattice constant c suggests a strong coupling between the spin and lattice ("magneto-elastic" coupling) in Cr_2GaN. This is extremely alike the typical characteristics of Mn-based MAX material Mn_2CaC and MnNiGe, where the magnetostriction effect is accompanied with the coupling among spin, lattice and electrical transport properties.[7,8,17]

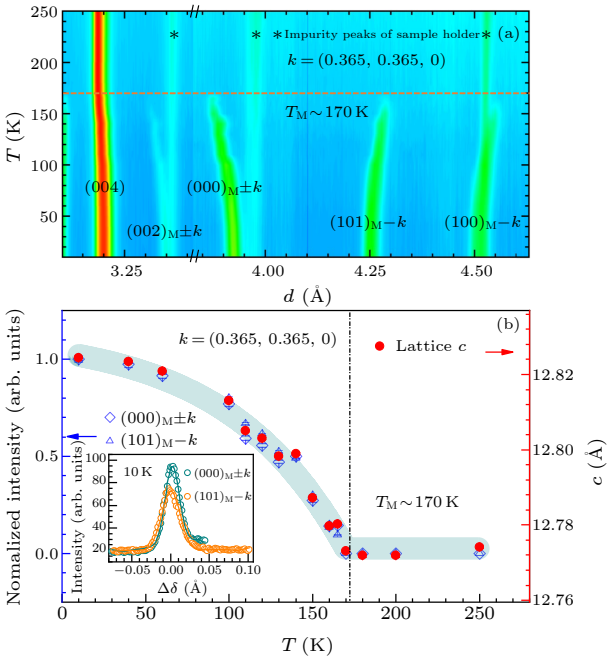

Fig. 3. (a) The temperature-dependent nuclear peak (004) and magnetic peaks of $(002)_M \pm k$, $(000)_M \pm k$, $(101)_M - k$, and $(100)_M - k$. (b) Temperature dependence of the normalized intensity of magnetic peaks $(000)_M \pm k$ and $(101)_M - k$ and lattice constant c. The inset in Fig. 3(b) is the fitting of magnetic peaks at 10 K. For these magnetic peaks, the fits to Gauss function are performed for different temperatures, and the obtained area represent their intensity of magnetic peaks.

Recent research has suggested the potential for the practical application of the MAX phases. The challenges in the immediate future are to further explore and characterize the MAX phases reported so far and to make further advance in boosting their industrial application. Here, the

presented experimental results show that Cr_2GaN exhibits a magnetic transition at 170 K, below which all Cr atoms are aligned with sinusoidal modulated magnetic structure. Accompanied with this magnetic transition, drastic change in the crystal structure of the material takes place, where 0.4% contraction in the out-of-plane c axis with increasing temperature from 10 K to 170 K indicates that it is a considerably large effect compared to what has commonly been observed in magnetostriction systems. The reported magneto-elastic coupling in Cr_2GaN is much like that in Mn-based MAX phase Mn_2GaC, in which the anisotropic structural changes are argued to be driven by magnetism.[8] For Cr_2GaN, by simply stretching the lattice in the c direction, the Cr–Cr interlayer distance is altered and thereby weakening magnetic coupling across the Ga layer, thus it becomes available to be capable of shifting the occurrence of magnetic transitions, as reported by doping and pressure effects in this compound.[12] Due to the magneto-elastic coupling interaction, it would be interesting for further studies to explore possible anisotropic response of the lattice and electrical conductivity to magnetic fields applied parallel and perpendicular to the c axis. Therefore, the single crystals of Cr_2GaN are highly desired for transport experiments to explore possible magnetoelectric or magnetocaloric applications.

Moreover, Cr_2GaN may be a candidate for topological magnetic texture or electronic states under its complex and tunable magnetism. To date, many novel magnetic topological materials, such as Co_2MnGa,[18–20] Co_2MnAl,[21,22] Co_2TiX ($X =$ Si, Ge and Sn),[23] XCo_2Z ($X =$ ⅣB or VB; $Z =$ ⅣA or ⅢA),[24] $Co_3Sn_2S_2$,[25,26] and $SrRuO_3$,[27,28] have been identified by combining topology of electronic band structures with magnetic configurations. These novel materials exhibit rich topological states due to strong spin-orbit coupling or magneto-elastic coupling, referred such as magnetic topological insulators, Weyl and Dirac magnetic semimetals, axionic insulators or higher-order topological phases of matter.[29–36] For Cr_2GaN as a 211-type compound similar to those Co-based systems, if the topological states exist, it will be very interesting to tune the topological states by its crystal structure continuously regulated by magnetism upon decreasing temperature.

In conclusion, the neutron powder diffraction and Rietveld refinement are carried out to determine the magnetic structure of Cr_2GaN, which is described as an incommensurate sinusoidal modulated structure with propagating vector $k = (0.365, 0.365, 0)$. Temperature-dependent diffraction patterns manifest that no structural transition occurs, but a c-axis lattice stretching below the magnetic phase transition temperature $T_M \approx 170$ K, which shows a similar behavior with the magnetic order parameter. The reported magneto-elastic coupling interplay in Cr_2GaN will provide us a platform for further exploring the possible magnetoelectric, magnetostrictive, magnetocaloric effects and magnetic topological states in the MAX compounds.

Acknowledgments. This work was supported by the National Natural Science Foundation of China (Grant Nos. 11822411, 12061130200, 11961160699, 11974392, and 52101236), the National Key Research and Development Program of China (Grant Nos. 2018YFA0704200, 2017YFA0303100, and 2020YFA0406003), the Strategic Priority Research Program (B) of the CAS (Grant No. XDB25000000), K. C. Wong Education Foundation (Grant No. GJTD-2020-01), the Youth Innovation Promotion Association of the CAS (Grant No. Y202001), Beijing Natural Science Foundation (Grant No. JQ19002), and the Newton Advanced Fellowship funding from the Royal Society of UK (Grant No. NAF\R1\201248). This work is based on neutron diffraction experiments performed at OSIRIS (Proposal No. RB1610019), ISIS Facility, Rutherford Appleton Laboratory, UK and WOMBAT (Proposal No. P6014), Australian Centre for Neutron Scattering, Australian Nuclear Science and Technology Organisation, Australia.

References

[1] Barsoum M W 2000 *Prog. Solid State Chem.* **28** 201
[2] Eklund P *et al.* 2010 *Thin Solid Films* **518** 1851
[3] Sun Z M 2011 *Int. Mater. Rev.* **56** 143
[4] Barsoum M W *et al.* 2001 *Am. Sci.* **89** 334
[5] Barsoum M W *et al.* 1996 *J. Am. Ceram. Soc.* **79** 1953
[6] Ingason A S, Dahlqvist M, and Rosen J 2016 *J. Phys.: Condens. Matter* **28** 433003
[7] Novoselova I P *et al.* 2018 *Sci. Rep.* **8** 2637
[8] Dahlqvist M *et al.* 2016 *Phys. Rev. B* **93** 014410
[9] Boucher R, Berger O, and Leyens C 2016 *Surf. Eng.* **32** 172
[10] Salikhov R *et al.* 2015 *Mater. Res. Lett.* **3** 156
[11] Liu Z, Waki T, Tabata Y, and Nakamura H 2014 *Phys. Rev. B* **89** 054435
[12] Li Y F, Liu J Z, Liu W H, Zhu X Y, and Wen H H 2015 *Philos. Mag.* **95** 2831
[13] Liu Z, Waki T, Tabata Y, Yuge K, Nakamura H, and Watanabe I 2013 *Phys. Rev. B* **88** 134401
[14] Rietveld H M 1969 *J. Appl. Crystallogr.* **2** 65
[15] Rodríguez-Carvajal J 1993 *Phys. B: Condens. Matter* **192** 55
[16] Wills A S 2000 *Physica B* **276–278** 680
[17] Ren Q Y, Hutchison W D, Wang J L, Studer A J, and Campbell S J 2018 *Chem. Mater.* **30** 1324
[18] Akito S *et al.* 2018 *Nat. Phys.* **14** 1119
[19] Manna K *et al.* 2018 *Phys. Rev. X* **8** 041045
[20] Guin S N *et al.* 2019 *NPG Asia Mater.* **11** 16
[21] Vilanova V E, Stryganyuk G, Schneider H, Felser C, and Jakob G 2011 *Appl. Phys. Lett.* **99** 132509
[22] Li P G *et al.* 2020 *Nat. Commun.* **11** 3476
[23] Chang G Q *et al.* 2016 *Sci. Rep.* **6** 38839
[24] Wang Z J *et al.* 2016 *Phys. Rev. Lett.* **117** 236401
[25] Liu C *et al.* 2021 *Sci. Chin. Phys. Mech. & Astron.* **64** 217062
[26] Liu C *et al.* 2021 *Sci. Chin. Phys. Mech. & Astron.* **64** 257511
[27] Itoh S *et al.* 2016 *Nat. Commun.* **7** 11788
[28] Jenni K *et al.* 2019 *Phys. Rev. Lett.* **123** 017202
[29] Xu Y F *et al.* 2020 *Nature* **586** 702
[30] Wang P Y, Ge J, Li J H, Liu Y Z, Xu Y, and Wang J 2021 *Innovation* **2** 100098
[31] Bernevig B A, Felser C, and Beidenkopf H 2022 *Nature* **603** 41
[32] Wang H *et al.* 2020 *Sci. Chin. Phys. Mech. & Astron.* **63** 287411
[33] Xie X C 2021 *Sci. Chin. Phys. Mech. & Astron.* **64** 217061
[34] Yan B H 2021 *Sci. Chin. Phys. Mech. & Astron.* **64** 217063
[35] Cai Z W *et al.* 2020 *Phys. Rev. B* **104** L020402
[36] Li J, Feng J S, Wang P S, Kan E J, and Xiang H J 2021 *Sci. Chin. Phys. Mech. & Astron.* **64** 286811